Supplemental Information

Germ cell-specific eIF4E1b regulates maternal mRNA translation to ensure zygotic genome activation

Guanghui Yang*, Qiliang Xin*, Iris Feng**, Di Wu*** and Jurrien Dean

Laboratory of Cellular and Developmental Biology, NIDDK,
National Institutes of Health, Bethesda, MD 20892, USA

* These authors contributed equally to this work
** Present address: Columbia University Vagelos College of Physicians and Surgeons, New York, NY 10032, USA
*** Present address: Janelia Research Campus, Howard Hughes Medical Institute, Ashburn, VA 20147, USA

Corresponding authors: jurrien.dean@nih.gov (J.D.); qiliang.xin@nih.gov (Q.X.)

This PDF file includes:
Supplemental Figures S1 to S11.
Other Supplemental Materials for this manuscript include the following:
Supplemental Tables S1 to S10.

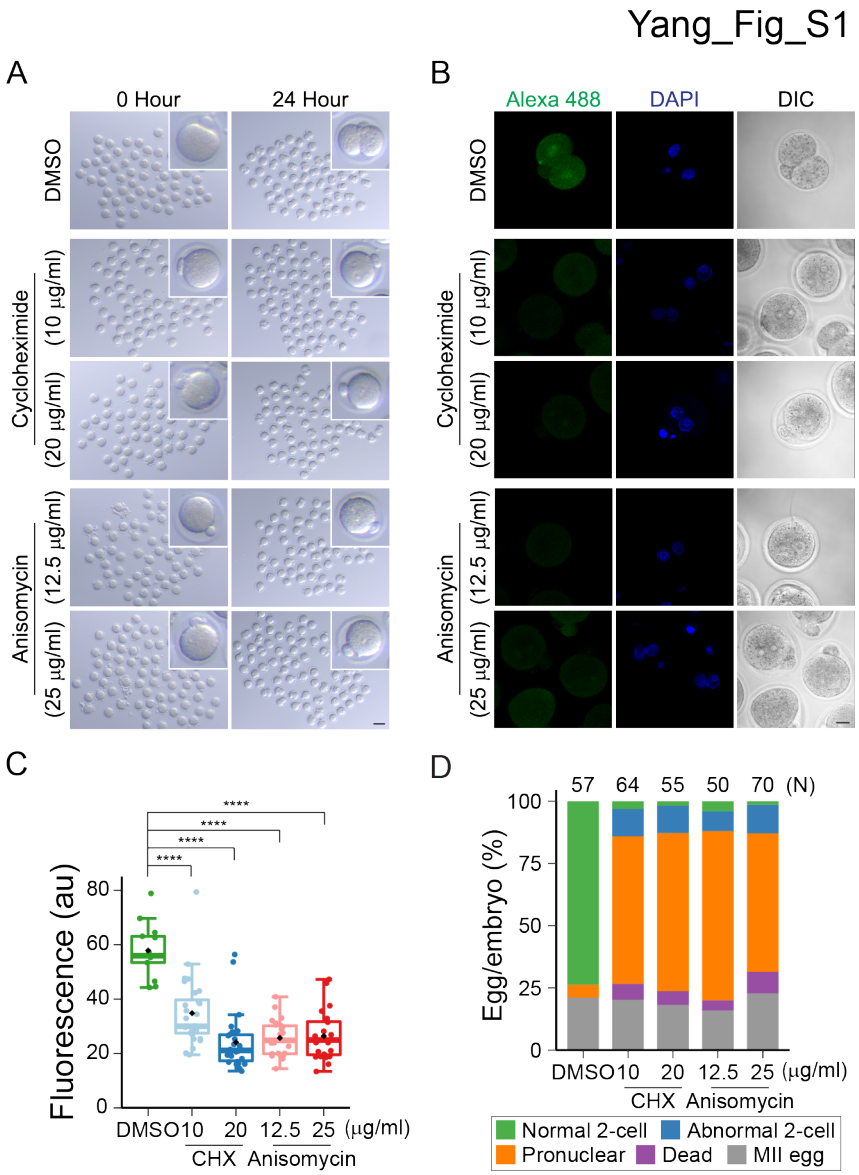

Supplemental Figure S1. Inhibition of maternal mRNA translation prevents mouse zygotic development. (*A*) Imaging MII eggs (0 Hour) before in vitro fertilization (IVF) and embryos after IVF and drug treatment (24 Hour). Inset shows one enlarged representative egg/embryo (4.5× magnification). Scale bar, 100 µm. (*B*) Imaging nascent proteins 24 h after IVF. Representative images are shown. Inhibition of protein synthesis arrested embryos at the pronuclear stage while control embryos progressed to two cells 24 h after insemination. Scale bar, 20 µm. (*C*) Qualification of fluorescence signal in all embryos examined in *B*. The box plot includes the median (horizontal line) and data between the 25th and 75th percentile and each dot reflects the signal in one embryo. The black diamonds show average within each group. (****) $P < 0.0001$; two-tailed *t*-test. (*D*) Ratio of embryos at different developmental stages with or without treatment 24 h after IVF. 4 h after insemination in IVF, embryos were washed and cultured in medium containing protein synthesis inhibitor cycloheximide (CHX) or anisomycin for additional 20 h. DMSO was used as the control.

Yang_Fig_S2

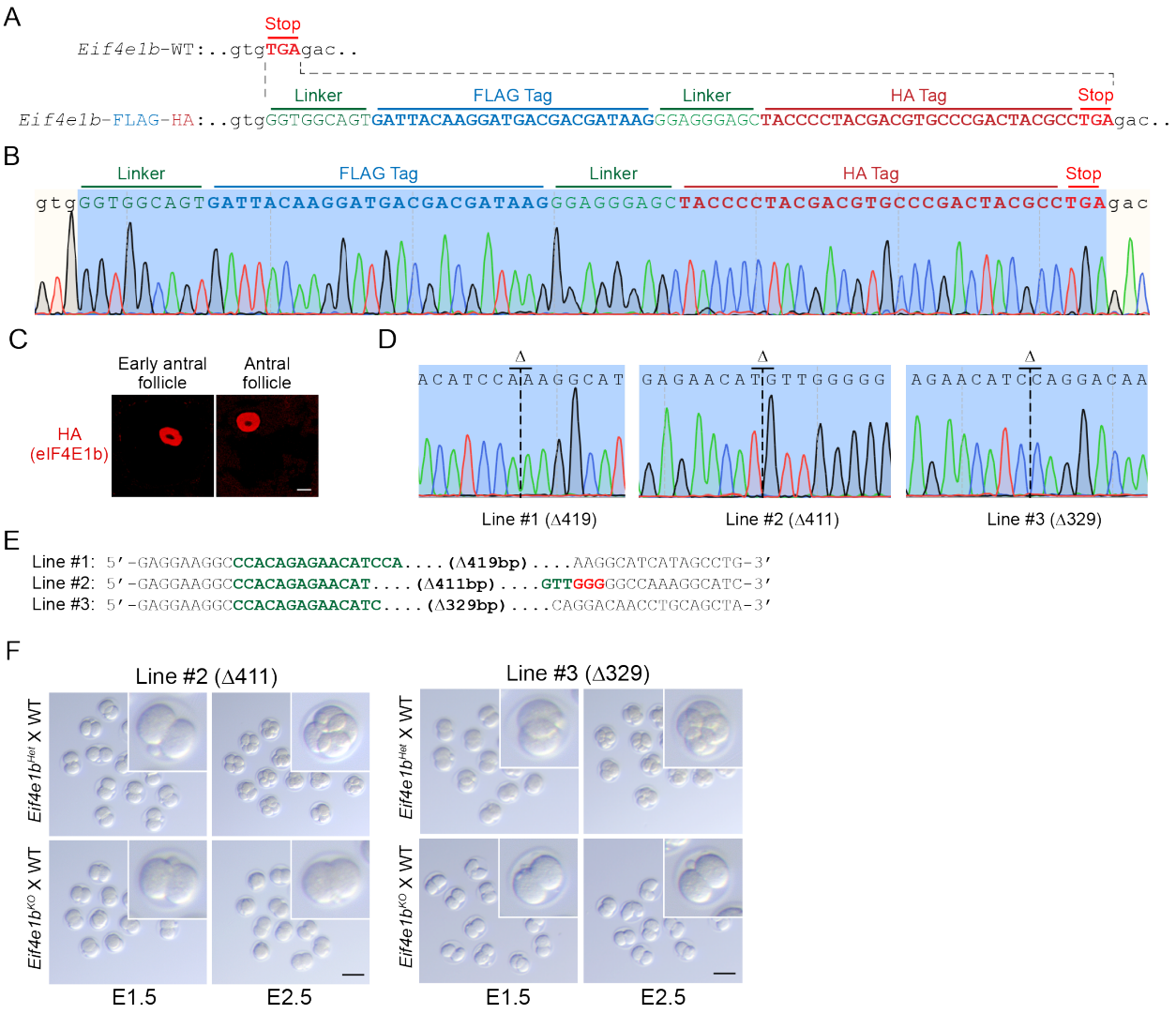

Supplemental Figure S2. *Eif4e1b* gene-edited mouse lines. (*A*) Design of the *Eif4e1b*^{KI} mouse line with FLAG and HA tags fused to Cterminus of the eIF4E1b protein. (*B*) Sanger sequencing at the *Eif4e1b*^{KI} locus of the knock-in (KI) mouse line. (*C*) 6-week *Eif4e1b*^{KI} mouse ovary sections (5 µm) were stained with anti-HA antibody to detect eIF4E1b protein in follicles. Scale bar, 50 µm. (*D*, *E*) Genomic sequences at the *Eif4e1b* locus in 3 different *Eif4e1b*^{KO} mouse lines with deletions ranging from 329 to 419 bp. (*F*) In vitro culture of embryos recovered from *Eif4e1b*^{KO} line #2 (Δ411) and line #3 (Δ329) female mice after successful mating with WT males. *Inset* magnification, 2.7×. Scale bar, 100 µm.

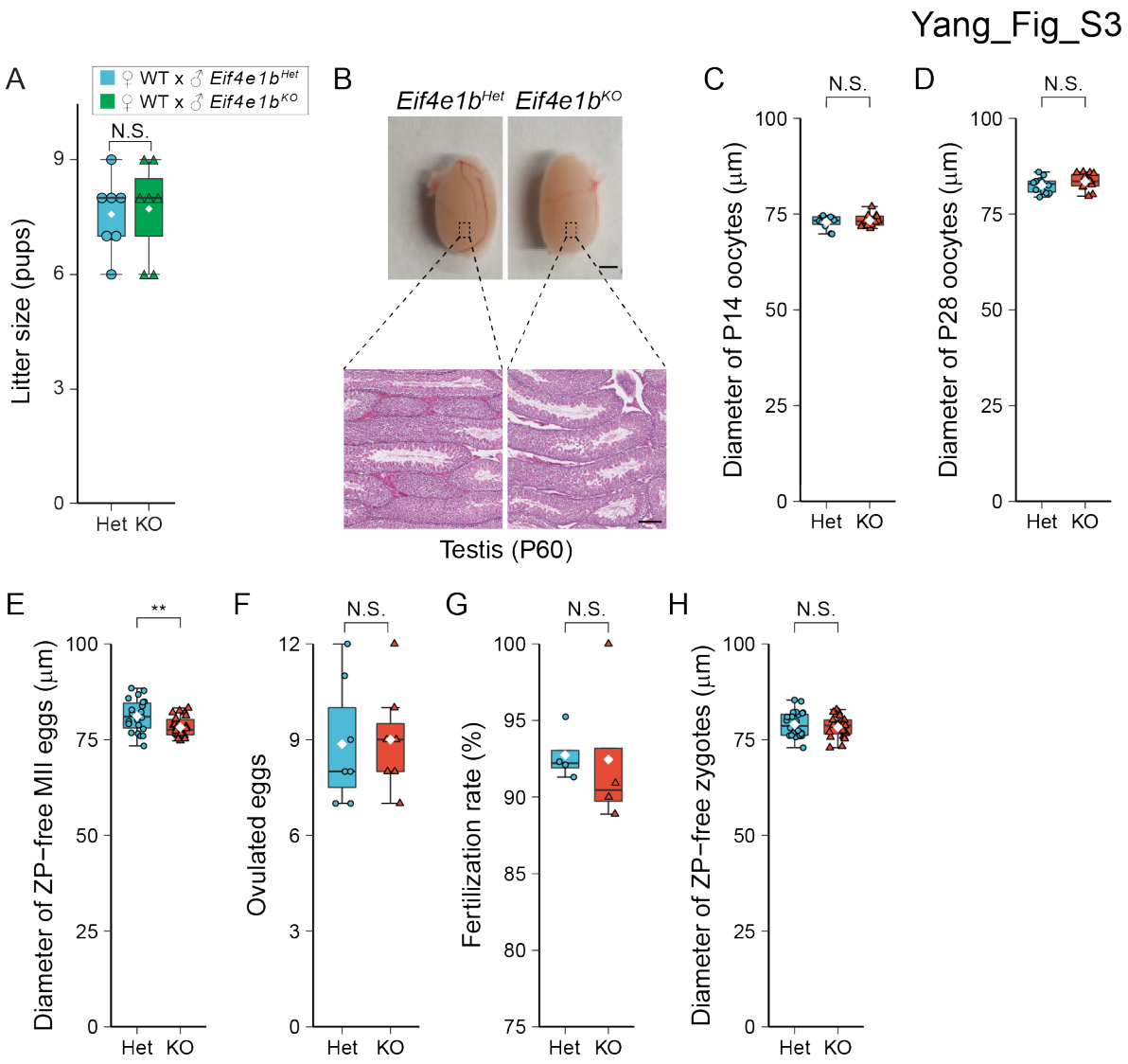

Supplemental Figure S3. Ablation of *Eif4e1b* does not affect male fertility or egg quality. (*A*) *Eif4e1b*^{Het} and *Eif4e1b*^{KO} male litter sizes after mating with WT female mice. (*B*) Morphology and histology of testes from *Eif4e1b*^{Het} and *Eif4e1b*^{KO} male mice at 2 mo. Scale bars, 2 mm (upper) and 50 μm (lower). (*C*) Diameter of oocytes collected from postnatal day 14 (P14) *Eif4e1b*^{Het} and *Eif4e1b*^{KO} female ovaries. (*D*) Same as *C*, but at P28. (*E*) Diameter of metaphase II (MII) eggs from *Eif4e1b*^{Het} and *Eif4e1b*^{KO} female mice. Zona pellucida was excluded when measuring the diameters. (*F*) Number of ovulated eggs from *Eif4e1b*^{Het} and *Eif4e1b*^{KO} female mice after normal mating. (*G*) In vitro fertilization rates of MII eggs collected from *Eif4e1b*^{Het} and *Eif4e1b*^{KO} female mice after insemination with WT epididymal sperm. (*H*) Diameter of fertilized zygotes from *Eif4e1b*^{Het} and *Eif4e1b*^{KO} female mice. Zona pellucida was excluded when measuring the diameters. (N.S.) not significant, (**) $P < 0.01$; two-tailed *t*-test.

Yang_Fig_S4

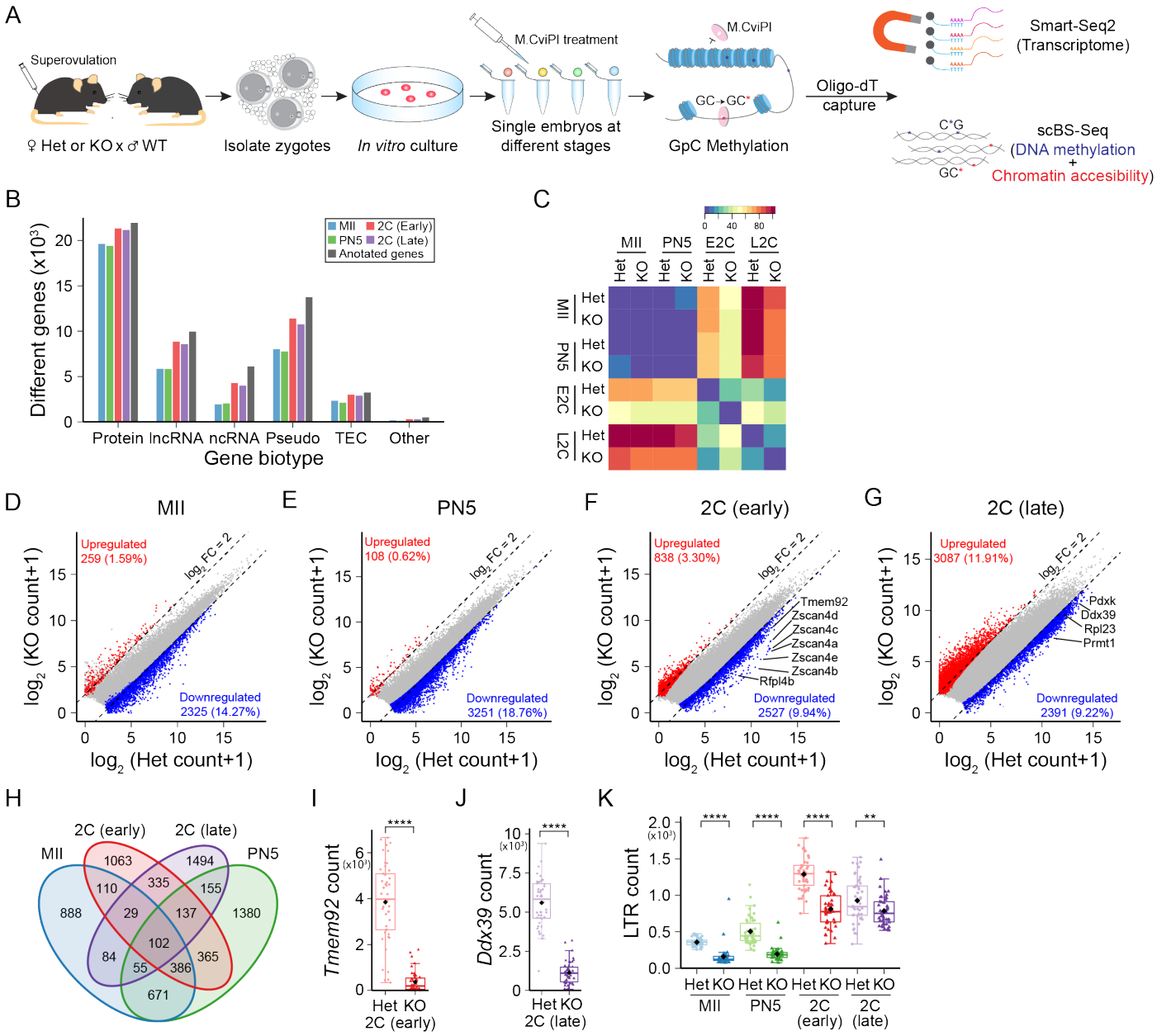
A
Superovulation
♀ Het or KO x ♂ WT
Isolate zygotes
In vitro culture
M.CviPI treatment
Single embryos at different stages
M.CviPI
GC→GC*
GpC Methylation
Oligo-dT capture
Smart-Seq2 (Transcriptome)
C*G
GC*
scBS-Seq (DNA methylation + Chromatin accesibility)
B
MII
2C (Early)
PN5
2C (Late)
Anotated genes
Different genes (x10³)
Protein
lncRNA
ncRNA
Pseudo
TEC
Other
Gene biotype
C
MII
PN5
E2C
L2C
Het
KO
D
MII
Upregulated 259 (1.59%)
Downregulated 2325 (14.27%)
E
PN5
Upregulated 108 (0.62%)
Downregulated 3251 (18.76%)
F
2C (early)
Upregulated 838 (3.30%)
Downregulated 2527 (9.94%)
Tmem92
Zscan4d
Zscan4c
Zscan4a
Zscan4e
Zscan4b
Rfpl4b
G
2C (late)
Upregulated 3087 (11.91%)
Downregulated 2391 (9.22%)
Pdxk
Ddx39
Rpl23
Prmt1
log2 FC = 2
log2 (KO count+1)
log2 (Het count+1)
H
MII
2C (early)
2C (late)
PN5
1063
1494
335
110
155
888
29
137
1380
102
84
55
386
365
671
I
Tmem92 count
Het KO
2C (early)
J
Ddx39 count
Het KO
2C (late)
K
LTR count
Het KO
MII
PN5
2C (early)
2C (late)

Supplemental Figure S4. Analyses of single embryo RNA-seq data. (*A*) Scheme of the single embryo (se) NMT-seq. *Eif4e1b*^{KO} and *Eif4e1b*^{Het} control females were hormonally stimulated and mated with wild type (WT) males. Zygotes were collected and cultured in vitro until the intended development stages. At the time of harvest, embryos were placed in lysis buffer containing the M. CviPI enzyme that could methylate all accessible GpC dinucleotides in the genome. Oligo-dT magnetic beads were used to capture RNA in the lysis and processed following the Smart-Seq2 protocol to obtain transcriptome profiles of single embryos. The genomic DNA remaining in the lysis was processed by the scBS (bisulfite)-seq protocol. The CpG methylation data from the scBS-seq reflected the DNA methylation profile in each embryo while the GpC methylation data was used to determine chromatin accessibility profiles. (*B*) Biotypes of RNAs detected by seRNA-seq. Protein, mRNA; lncRNA, long non-coding RNA; ncRNA, non-coding RNA; Pseudo, pseudogene RNA; TEC, to be experimentally confirmed. (*C*) Heatmap showing distances between different clusters of MII eggs and early embryos in the PCA plot of Fig. 3*A*. Note the smaller differences in MII and PN5 samples, even between samples from *Eif4e1b*^{Het} and *Eif4e1b*^{KO} females. (*D*-*G*) Scatter plots documenting differentially expressed RNAs in MII eggs, PN5 zygotes and two-cell (2C) embryos. Up- and down-regulated RNAs are shown as red and blue dots, respectively. The total number of up- or down- regulated RNAs is labelled in each plot. mRNAs from multiple well-known ZGA genes are labeled in the plots of early and late two-cell embryos. (*H*) Venn diagram showing overlapping down-regulated genes detected in eggs (MII) and embryos (PN5, early and late 2C). (*I*) Abundance of *Tmem92*, a minor ZGA gene, in early two-cell embryos derived from *Eif4e1b*^{Het} and *Eif4e1b*^{KO} females. (*J*) Same as *I*, but for *Ddx39*, a major ZGA gene, at the late two-cell stage. (*K*) Abundance of transcripts from LTR transposons in embryos from eggs/embryos derived from *Eif4e1b*^{Het} and *Eif4e1b*^{KO} female mice at different developmental stages. (**) $P < 0.01$, (****) $P < 0.0001$; two-tailed *t*-test.

Yang_Fig_S5

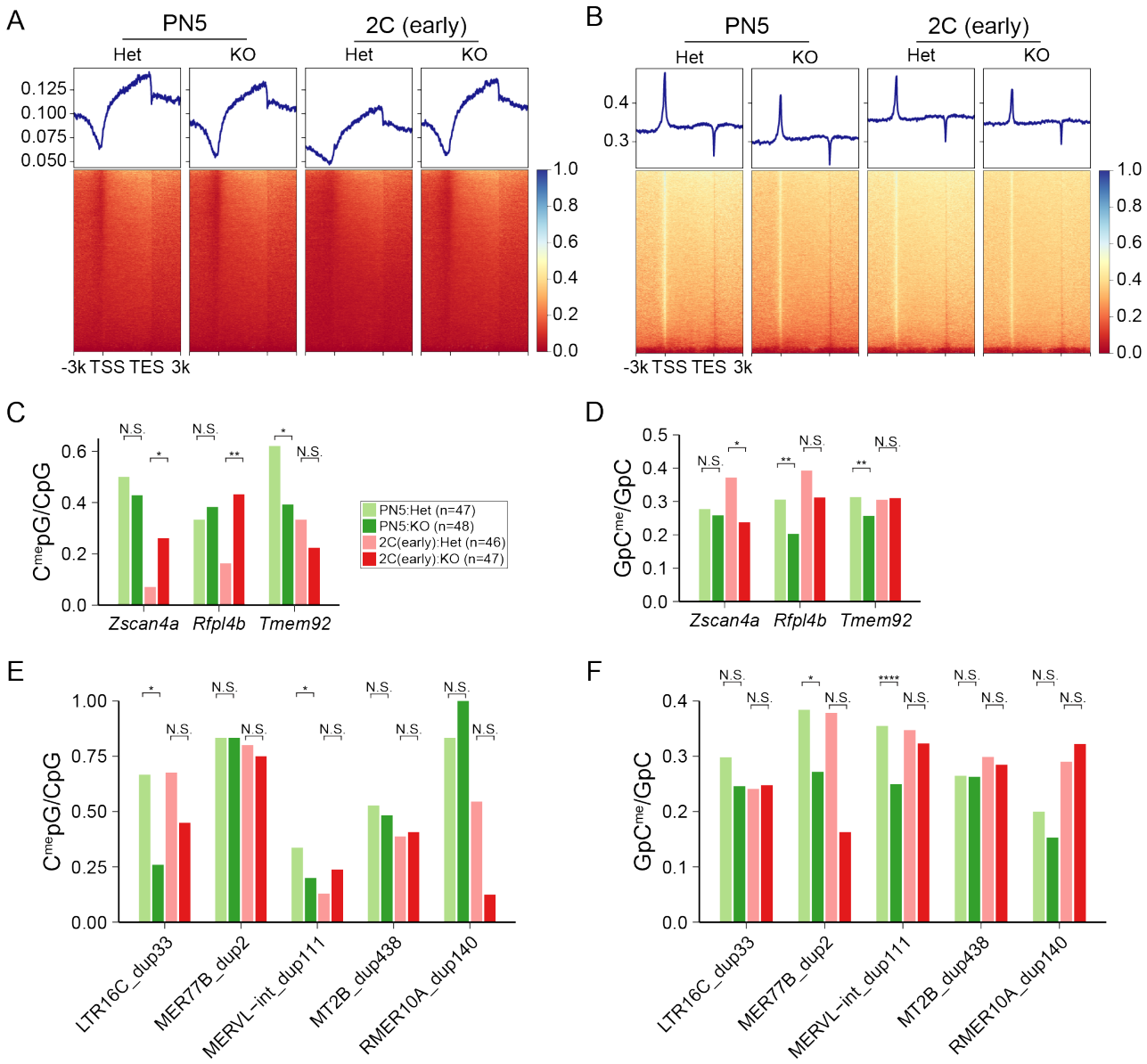
A
PN5
2C (early)
Het
KO
Het
KO
0.125
0.100
0.075
0.050
1.0
0.8
0.6
0.4
0.2
0.0
-3k TSS TES 3k
B
PN5
2C (early)
Het
KO
Het
KO
0.4
0.3
1.0
0.8
0.6
0.4
0.2
0.0
-3k TSS TES 3k
C
CmepG/CpG
N.S.
*
N.S.
**
*
N.S.
PN5:Het (n=47)
PN5:KO (n=48)
2C(early):Het (n=46)
2C(early):KO (n=47)
Zscan4a
Rfpl4b
Tmem92
D
GpCme/GpC
N.S.
*
N.S.
**
N.S.
**
Zscan4a
Rfpl4b
Tmem92
E
CmepG/CpG
LTR16C_dup33
MER77B_dup2
MERVL−int_dup111
MT2B_dup438
RMER10A_dup140
F
GpCme/GpC
N.S.
*
****
N.S.
LTR16C_dup33
MER77B_dup2
MERVL−int_dup111
MT2B_dup438
RMER10A_dup140

Supplemental Figure S5. DNA methylation and chromatin accessibility in embryos from control and *Eif4e1b*^{KO} female mice. (*A*) Global DNA methylation profiles around annotated genes in embryos from control and *Eif4e1b*^{KO} female mice. (*B*) Same as *A*, but for chromatin accessibility. (*C*) DNA methylation levels in the promoter and gene body regions of *Zscan4a*, *Rfpl4b*, *Tmem92* (3 minor ZGA genes) in PN5 and early two-cell embryos from control and *Eif4e1b*^{KO} female mice. (*D*) Same as *C*, but for chromatin accessibility. (*E*, *F*) Similar to *C* and *D* but at transposon gene loci. When individual genes/transposons are examined in *C*-*F*, DNA-seq data of samples from the same developmental stage with the same strain for PN5 (47 Het, 48 KO) and early two-cell (46 Het, 47 KO) embryos are merged to obtain the ratio of methylated CpG or GpC under each experimental condition. Each embryo represents an independent biological replicate. To test ratio equality of methylated- CpG and GpC under different experimental conditions, the two-sided proportion test function from R was used to calculate P values: (N.S.) not significant, (∗) $P < 0.05$, (∗∗) $P < 0.01$, (∗∗∗∗) $P < 0.0001$.

Yang_Fig_S6

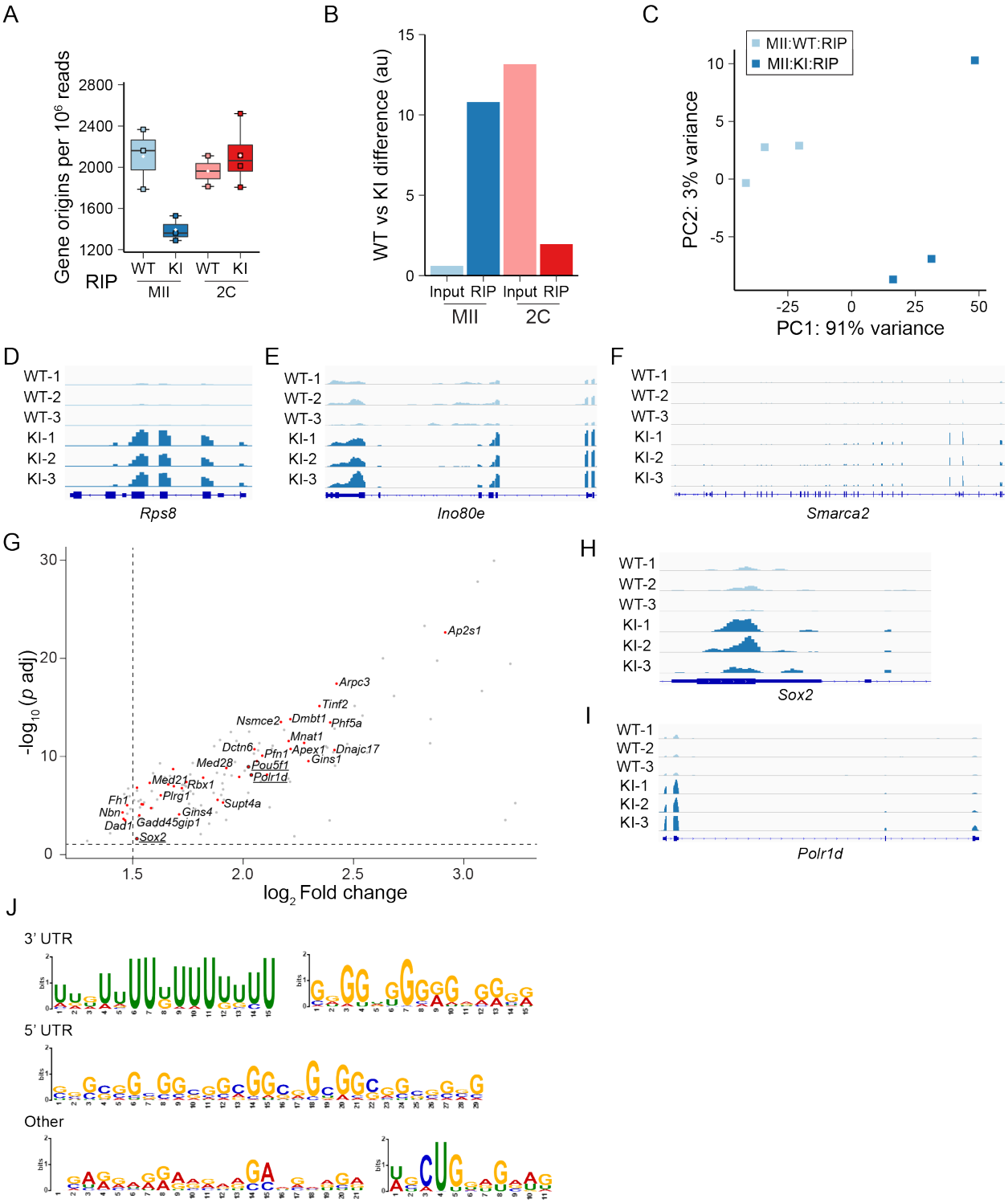
A
Gene origins per 10^6 reads
2800
2400
2000
1600
1200
RIP
WT KI WT KI
MII 2C
B
WT vs KI difference (au)
15
10
5
0
Input RIP Input RIP
MII 2C
C
MII:WT:RIP
MII:KI:RIP
PC2: 3% variance
10
5
0
-5
-25 0 25 50
PC1: 91% variance
D
WT-1
WT-2
WT-3
KI-1
KI-2
KI-3
Rps8
E
Ino80e
F
Smarca2
G
-log10 (p adj)
30
20
10
0
1.5 2.0 2.5 3.0
log2 Fold change
Ap2s1
Arpc3
Tinf2
Nsmce2
Dmbt1
Phf5a
Mnat1
Dctn6
Pfn1
Apex1
Dnajc17
Gins1
Med28
Pou5f1
Pdlr1d
Med21
Rbx1
Plrg1
Fh1
Supt4a
Nbn
Gins4
Dad1
Gadd45gip1
Sox2
H
Sox2
I
Polr1d
J
3' UTR
5' UTR
Other

Supplemental Figure S6. Analyses of RIP-seq data. (*A*) Gene origins per million reads from the RIP-seq data. (*B*) Length of the dashed lines in Fig. 5*A* showing differences between two group of samples. Variances of PC1 and PC2 are used for the calculation. (*C*) Principal component analysis (PCA) of input and RIP-seq data from MII eggs. Note: The X axis captured almost all variance and embryos from the same genotype are close together while embryos from different genotypes are at a distance. (*D-F*) Integrated genomic view (IGV) of eIF4E1b RIP-seq results at *Rps8*, *Ino80e*, *Smarca2* gene loci in sequencing data from WT and *Eif4e1b*^{KI} MII eggs. (*G*) Part of the volcano plot showing only transcripts function during embryogenesis and observed in RIP-seq. Each dot represents one transcript and those expressed during preimplantation development are red and labeled. *Sox2*, *Oct4*(*Pou5f1*) and *Polr1d* are also targets of eIF4E1b. (*H*, *I*) Integrated genomic view (IGV) of eIF4E1b RIP-seq results at *Sox2* and *Polr1d* gene loci in RIP-seq data from WT and *Eif4e1b*^{KI} MII eggs. (*J*) Motifs shared by eIF4E1b RNA targets. 2 motifs at the 3' UTR, 1 motif at the 5' UTR and 2 other shared motifs are shown as identified by MEME software suite.

Yang_Fig_S7

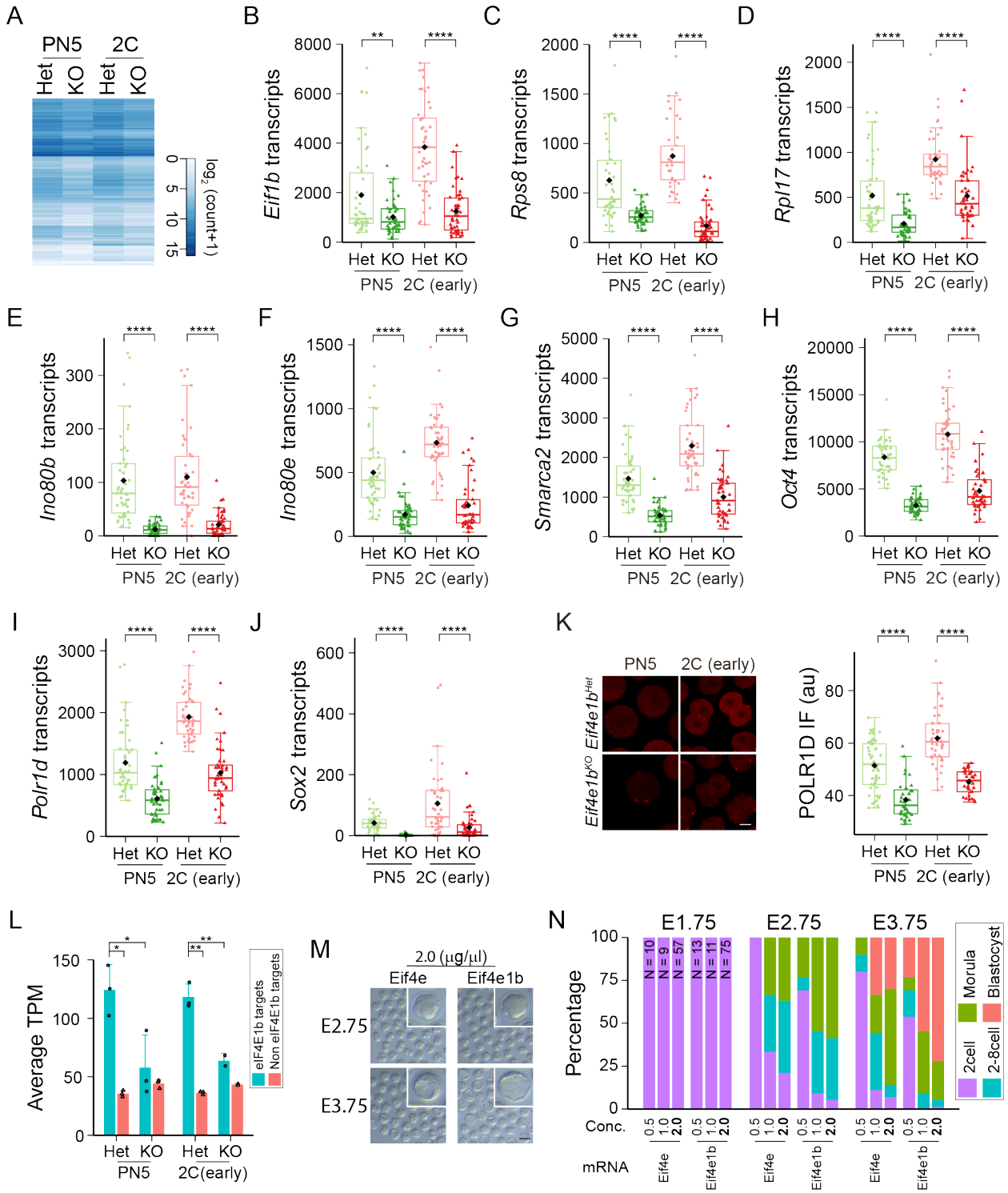
A
PN5
2C
Het
KO
Het
KO
log2 (count+1)
0
5
10
15
B
Eif1b transcripts
C
Rps8 transcripts
D
Rpl17 transcripts
E
Ino80b transcripts
F
Ino80e transcripts
G
Smarca2 transcripts
H
Oct4 transcripts
I
Polr1d transcripts
J
Sox2 transcripts
K
PN5
2C (early)
Eif4e1b^Het
Eif4e1b^KO
POLR1D IF (au)
L
Average TPM
eIF4E1b targets
Non eIF4E1b targets
Het KO Het KO
PN5 2C(early)
M
2.0 (μg/μl)
Eif4e
Eif4e1b
E2.75
E3.75
N
E1.75
E2.75
E3.75
Percentage
N = 10
N = 9
N = 57
N = 13
N = 11
N = 75
Morula
Blastocyst
2cell
2-8cell
Conc.
mRNA
Eif4e
Eif4e1b

Supplemental Figure S7. eIF4E1b regulates expression of its maternal mRNA targets. (*A*) Heatmap showing average expression of eIF4E1b mRNA targets in embryos from *Eif4e1b*^{Het} and *Eif4e1b*^{KO} females at different developmental stages as determined by single embryo RNA-seq. All counts were normalized by ERCC spike-in. (*B-J*) Abundance of *Eif1b*, *Rps8*, *Rpl17*, *Ino80b*, *Ino80e*, *Smarca2*, *Oct4*(*Pou5f1*), *Polr1d* and *Sox2* in zygotes and early two-cell embryos from control and *Eif4e1b*^{KO} female mice as determined by single embryo RNA-seq. Note *Eif4e1b* maternal deletion leads to accelerated degradation of these RNAs due to lose of binding and protection. (*K*) POLR1D protein expression in PN5 zygotes and early two-cell embryos from *Eif4e1b*^{Het} and *Eif4e1b*^{KO} females. Scale bar, 20 μm. The fluorescent signals are quantified to show decreased expression from the maternal *Polr1d* mRNA after maternal deletion of *Eif4e1b*. (∗∗) $P < 0.01$, (∗∗∗∗) $P < 0.0001$; two-tailed *t*-test. (*L*) Low input Ribo-seq results using PN5 zygotes and early 2-cell embryos from *Eif4e1b*^{Het} and *Eif4e1b*^{KO} female mice. eIF4E1b targets bind more ribosomes in *Eif4e1b*^{Het} control females and their ribosome binding ability is reduced after maternal ablation of *Eif4e1b*. Unique mapped reads from protein-coding transcripts that were also protected by ribosomes were used for analysis. Average TPM values of eIF4E1b mRNA targets and non-targets were calculated in each sample and used for plotting. (∗) $P < 0.05$, (∗∗) $P < 0.01$; two-tailed *t*-test. (*M*) Morphology of in vitro cultured embryos after microinjecting higher dose (2.0 μg/μl) *Eif4e* or *Eif4e1b* mRNAs into zygotes from *Eif4e1b*^{KO} females. The percentage of embryos at different developmental stages is quantified in *N*. *Inset* magnification, 2.8×. Scale bar, 100 μm.

Yang_Fig_S8

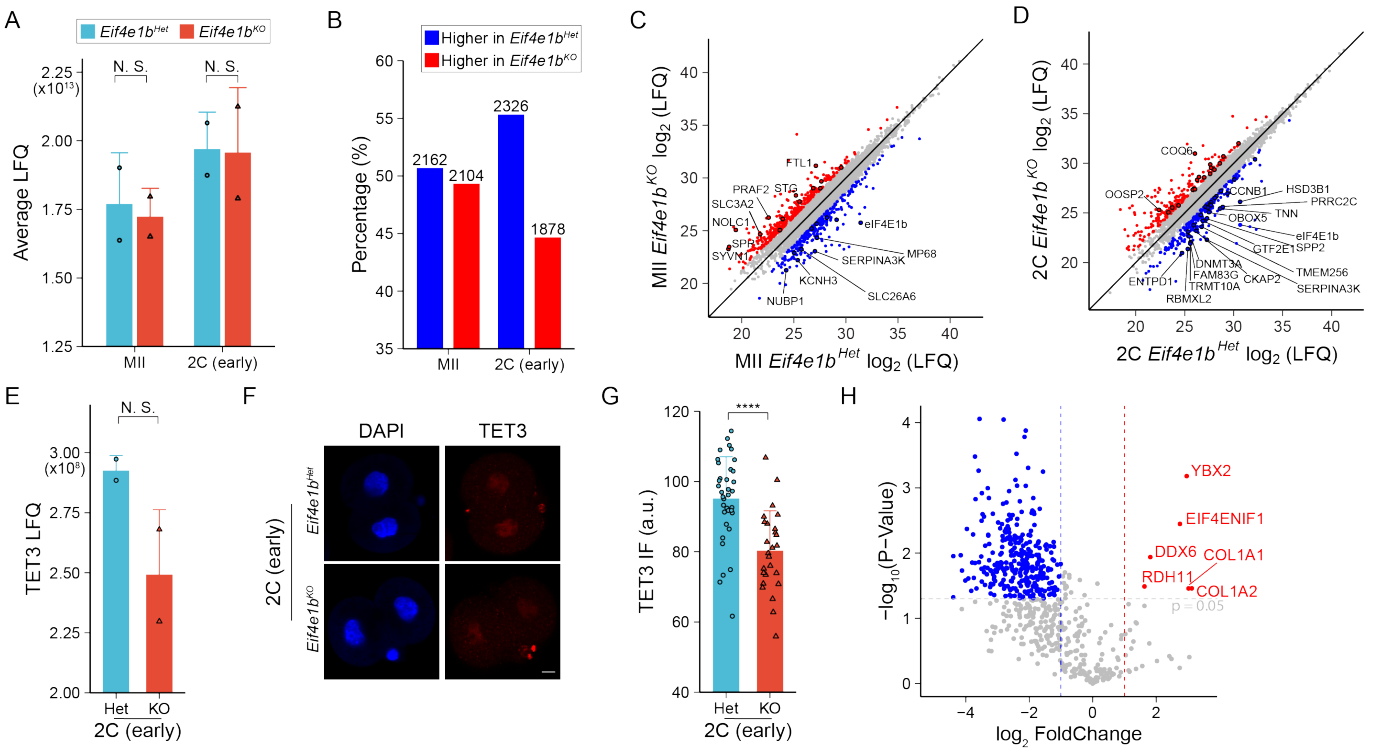

Supplemental Figure S8. Analyses of mass spectrometry results. (*A*) Bar plot showing the average of total label-free quantification (LFQ) values and standard deviations of samples in the same group after analysis of low-input mass spectrometry data. Sum of LFQ values of each sample is labeled as a dot or triangle. (N.S.) not significant, two-tailed *t*-test. (*B*) Percentage of proteins that are higher expressed in *Eif4e1b*^{Het} or *Eif4e1b*^{KO} samples. Total number of proteins is labeled *above* each bar. (*C*, *D*) Global view of protein expression in eggs/embryos from *Eif4e1b*^{Het} and *Eif4e1b*^{KO} female mice. Proteins that have more than 2-fold changes in LFQ values between Eif*4e1b*^{Het} and *Eif4e1b*^{KO} samples are labeled in red or blue. The ones which also have P value < 0.1 in two-tailed *t*-test are labeled by black circles. Names of proteins that have fold change > 3 are labeled. Note that more proteins are down-regulated in *Eif4e1b*^{KO} early two-cell embryos. (*E*) TET3 expression level in early two-cell embryos as determined in the low-input mass spectrometry. (N.S.) not significant, two-tailed *t*-test. (*F*) Immunostaining of TET3 in early two-cell embryos from *Eif4e1b*^{Het} and *Eif4e1b*^{KO} female mice. The IF signal from multiple embryos is quantified in *G*. Scale bar, 10 μm. (****) P < 0.0001; two-tailed *t*-test. (*H*) Volcano plot using eIF4E1b^{HA} IP and LC-MS/MS results. Ovary lysates of *Eif4e1b*^{KI} and WT female mice were analyzed. Potential eIF4E1b binding patterners are labeled red.

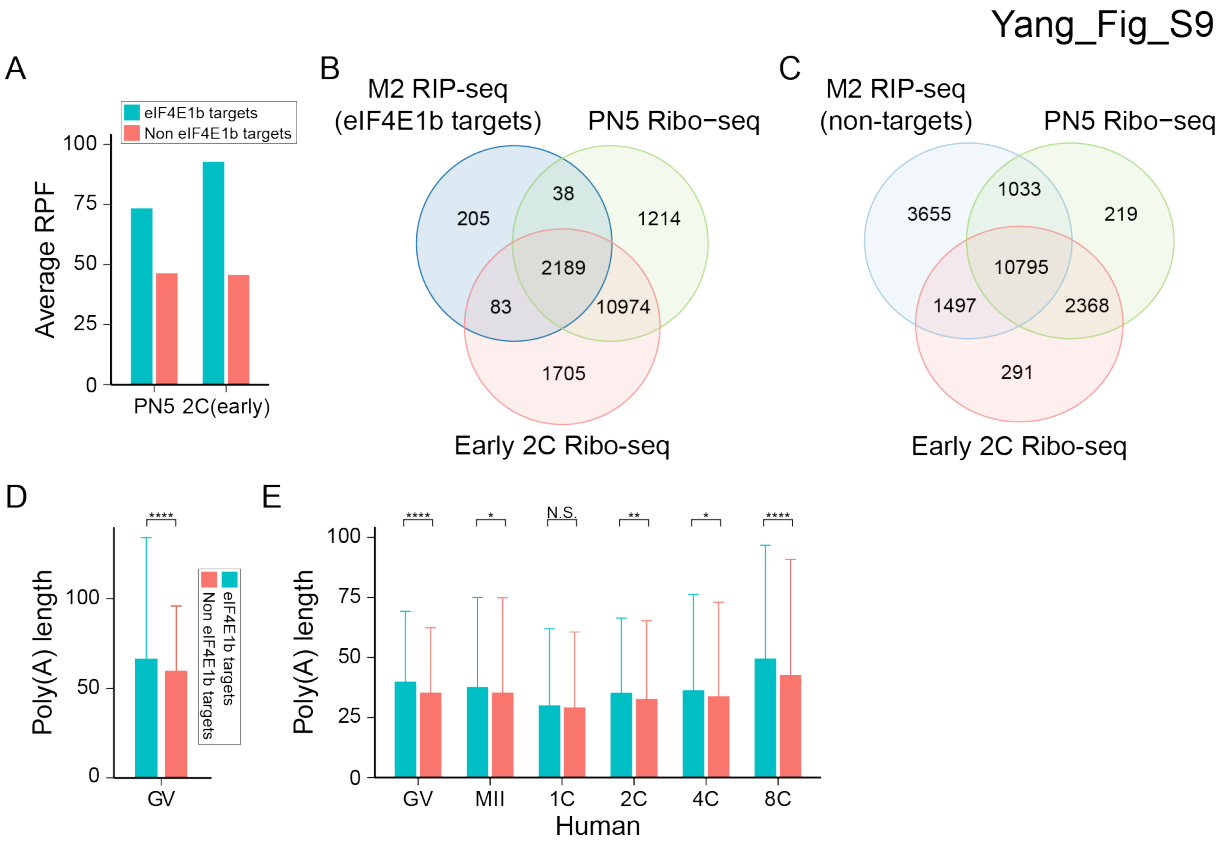

Supplemental Figure S9. eIF4E1b RNA targets have higher ribosome binding and longer poly(A) tails. (*A*) Average of ribosome protected fragments (RPF) of two groups of transcripts as determined by Ribo-seq in WT embryos. Note transcripts that are identified as eIF4E1b targets in this study show higher ribosome binding both in PN5 zygotes and early two-cell embryos which could facilitate their translation. (*B*) Venn diagram to show number of overlapping mRNAs that were determined as eIF4E1b targets in MII RIP-seq with those detected to bind ribosomes in PN5 zygotes and early two-cell (2C) embryos in Ribo-seq. (*C*) Same as *B*, but for non-eIF4E1b targets. Larger ratio of eIF4E1b maternal mRNA targets maintain binding to ribosomes at these stages, suggesting active translation. (*D*) Average poly(A) tail length of eIF4E1b targets and non-targets as determined by PAISO-seq using mouse GV oocytes. (*E*) Average poly(A) tail length of eIF4E1b targets and non-targets as determined by PAISO-seq using human oocytes/embryos at different developmental stages. Minor ZGA is detected at two-cell stage while major ZGA is detected at eight-cell stage in human embryos. eIF4E1b RNA targets have longer poly(A) tails. (N.S.) not significant, (*) $P < 0.05$, (**) $P < 0.01$, (****) $P < 0.0001$; two-tailed *t*-test.

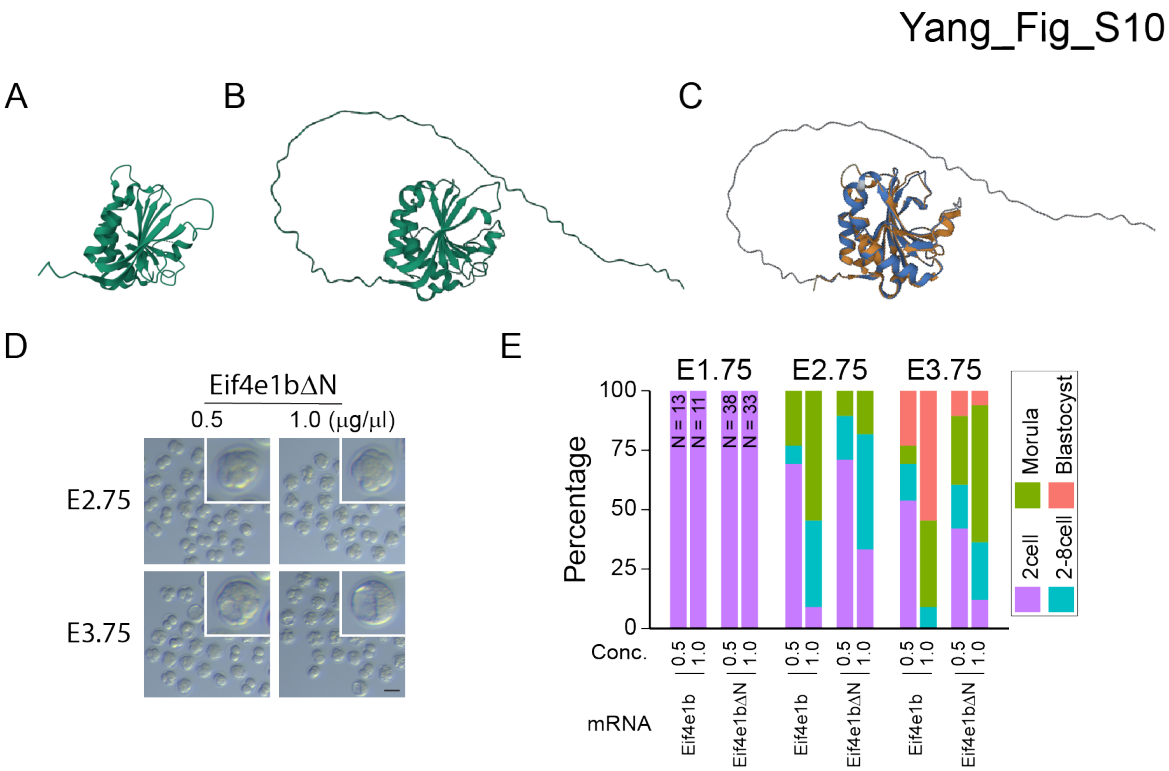

Supplemental Figure S10. Structure and function related to the N terminal domain of eIF4E1b. (*A*) Structure of eIF4E as determined by X-ray crystallography. (*B*) Structure of eIF4E1b as predicted by AlphaFold. (*C*) Alignment of structures in *A* and *B*. (*D*) Morphology of *in vitro* cultured embryos after microinjecting mRNAs of *Eif4e1bΔN*, a truncated form of *Eif4e1b* lacking 2-62 amino acids, into zygotes from *Eif4e1b*^{KO} female mice. The percentage of embryos at different developmental stages is quantified in *E*. *Inset* magnification, 2.8×. Scale bar, 100 μm.

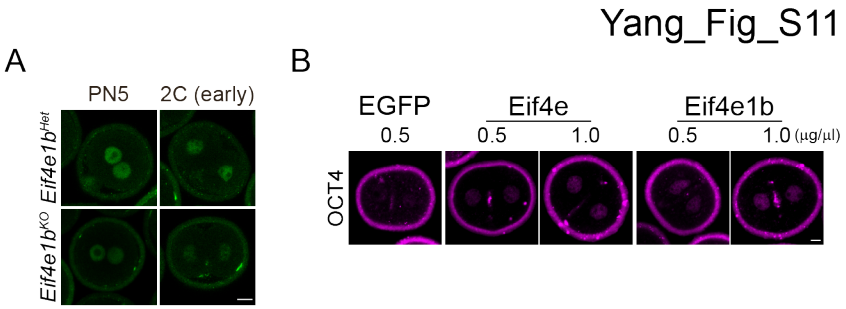

Supplemental Figure S11. Original images before removal of non-specific binding to zonae pellucidae. (*A*) Fig. 6*B* images prior to computational processing. (*B*) Fig. 6*G* images prior to computational processing.

Supplemental Tables S1 to S10 are included as separate Excel (.xlsx) files.
Supplemental Table S1. Normalized mean counts of all annotated genes at different stages of different strains.
Supplemental Table S2. Minor ZGA genes used for analysis.
Supplemental Table S3. Major ZGA genes used for analysis.
Supplemental Table S4. Normalized mean counts of all annotated transposable elements at different stages of different strains.
Supplemental Table S5. Differential gene expression analysis using MII egg RIP-seq data.
Supplemental Table S6. Normalized counts of RNAs coding histone modifiers and subunits of chromatin remodeling complexes in RIP-seq using MII eggs.
Supplemental Table S7. LFQ results of low-input mass spectrometry.
Supplemental Table S8. Processed ovary IP-LC/MS results.
Supplemental Table S9. Primers and oligos.
Supplemental Table S10. Source data for Fig. 2C,D; Fig. 6A,B,D,F,H,I; Supplemental Fig. S1C,D; Supplemental Fig. S3A,C-H; Supplemental Fig. S7K, Supplemental Fig. S8G .